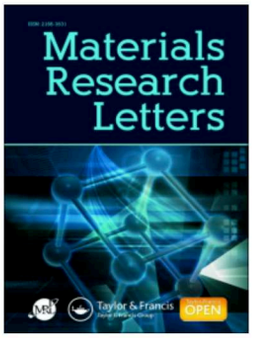

Materials Research Letters

ISSN: 2166-3831 (Online) Journal homepage: www.tandfonline.com/journals/tmrl20

Liquid metal embrittlement in solid-state welding of Mg/galvanized steel

Ting Chen, Hao Wang, Banglong Fu, Chunjie Huang, Tong Shen, Uceu F. H. R. Suhuddin, Emad Maawad, Thomas Klassen, Guoliang Qin & Benjamin Klusemann

To cite this article: Ting Chen, Hao Wang, Banglong Fu, Chunjie Huang, Tong Shen, Uceu F. H. R. Suhuddin, Emad Maawad, Thomas Klassen, Guoliang Qin & Benjamin Klusemann (2025) Liquid metal embrittlement in solid-state welding of Mg/galvanized steel, Materials Research Letters, 13:7, 785-792, DOI: 10.1080/21663831.2025.2516103

To link to this article: https://doi.org/10.1080/21663831.2025.2516103

MATER. RES. LETT.
2025, VOL. 13, NO. 7, 785–792
https://doi.org/10.1080/21663831.2025.2516103

MATERIALS RESEARCH LETTERS
Taylor & Francis
Taylor & Francis Group

ORIGINAL REPORT

Liquid metal embrittlement in solid-state welding of Mg/galvanized steel

Ting Chen[a*], Hao Wang[b*], Banglong Fu[a,b], Chunjie Huang[c], Tong Shen[a], Uceu F. H. R. Suhuddin[a], Emad Maawad[d], Thomas Klassen[c], Guoliang Qin[b] and Benjamin Klusemann[a,e]

[a]Solid State Materials Processing, Institute of Material and Process Design, Helmholtz-Zentrum Hereon, Geesthacht, Germany; [b]School of Materials Science and Engineering, Shandong University, Jinan, People's Republic of China; [c]Helmut Schmidt University, University of the Federal Armed Forces Hamburg, Hamburg, Germany; [d]Institute of Materials Physics, Helmholtz-Zentrum Hereon, Geesthacht, Germany; [e]Institute for Production Technology and Systems, Leuphana University Lüneburg, Lüneburg, Germany

ABSTRACT

The phenomenon of liquid metal embrittlement (LME) poses safety concerns for welded joints in the manufacturing field. In present study, LME was observed in refill friction stir spot welding (refill FSSW) of dissimilar magnesium (Mg) to galvanized steel. This marks the first reported proof of evidence of LME in the field of solid-state welding. Microstructural characterization of cracks formed during the welding process revealed typical characteristics of LME, specifically the penetration and enrichment of Zn at the Mg alloy grain boundaries and the formation of a liquefied phase. Tensile tests of Zn-coated Mg alloy were conducted at elevated temperatures to validate the LME phenomenon in refill FSSW and to identify the temperature range in which LME occurs. Based on these observations, a mechanism of LME formation for the Mg-Zn system in refill FSSW is proposed. Additionally, strategies to prevent LME are suggested and experimentally validated.

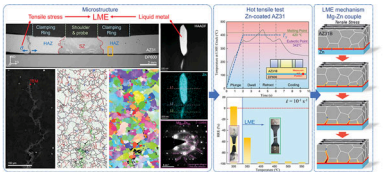

ARTICLE HISTORY
Received 6 March 2025

KEYWORDS
Liquid metal embrittlement; solid-state welding; refill friction stir spot welding; Mg alloys; Zn

Liquid metal embrittlement (LME) is a critical phenomenon that affects various structural materials, including steel [1–3], aluminum [4–6], brass [7,8], and nickel [9], particularly during high-temperature processes such as welding, hot deformation, brazing, heat treatment, and in-service operations. In industries like automotive, aerospace, and nuclear, LME is a significant safety concern due to its impact on material performance. LME occurs when a normally ductile material loses its ductility upon contact with a liquid metal, leading to brittle fracture under tensile stresses. This phenomenon arises from the combined effect of three factors [10]: (a) the presence of an aggressive liquid metal with a relatively low melting point, (b) a susceptible solid material prone to liquid metal penetration, and (c) the application of external or internal (residual) tensile stresses.

One of the most pressing LME concerns in the automotive industry is the increased use of zinc (Zn)-coated advanced high-strength steels (AHSS) in vehicle construction [11–13], particularly during resistance spot welding (RSW) [14–16]. During the RSW process, liquid Zn comes into contact with solid steel at both the joint sheet-to-sheet interface and the electrode/sheet interface. This contact occurs when temperatures rise above the Zn's melting point (419°C) but remain below the melting point of steel (~1475°C). The liquid Zn penetrates steel grain boundaries under the tensile stresses generated during welding, leading to the initiation and

CONTACT Ting Chen ting.chen@hereon.de Solid State Materials Processing, Institute of Material and Process Design, Helmholtz-Zentrum Hereon, Max-Planck-Str. 1, Geesthacht 21502, Germany; Banglong Fu bl.fu@sdu.edu.cn Solid State Materials Processing, Institute of Material and Process Design, Helmholtz-Zentrum Hereon, Max-Planck-Str. 1, Geesthacht 21502, Germany School of Materials Science and Engineering, Shandong University, Jingshi Road 17923, Jinan 250061, People's Republic of China
*These authors contributed equally to this work and should be considered co-first authors.

Supplemental data for this article can be accessed online at https://doi.org/10.1080/21663831.2025.2516103.

propagation of LME cracks [17]. It has been concluded that LME occurs at the temperature range of 700 ~ 900°C or below the melting point of steel [10]. Notably, LME was so far not observed in solid-state welding processes due to the lower welding temperatures involved [18,19].

The need to reduce vehicle weight while maintaining load capacity has led to the development of hybrid magnesium (Mg)/steel structures [20]. However, joining Mg to steel is challenging because the Mg/Fe system is immiscible, exhibiting almost no inter-solubility or reaction [21]. Zn coatings have been shown to improve the quality of Mg/steel welds by preventing oxidation and aiding the brazing process [22]. Nevertheless, these coatings also pose a risk of LME in Mg alloys, potentially compromising the mechanical properties of the welded joints. This study is the first to identify clearly LME in solid-state welding of Mg alloys to galvanized steel. It explores the underlying mechanism of LME in Mg-Zn couple and proposes strategies to prevent its occurrence.

The base materials (BM) used in this study were commercial AZ31B Mg alloy sheets with a thickness of 2 and 1.5 mm thick hot-dip galvanized DP600 steel sheets. To investigate the effects of Zn coating, the results are compared to bare DP600 steel. The BM (Mg/Steel) were welded by refill friction stir spot welding (refill FSSW). The tool system and the procedure of refill FSSW are presented in Figure 1(a) and (b). The tool system consists of a clamping ring (diameter of 14.5 mm), a shoulder (9 mm) and a probe (6 mm). It was assembled on the RPS200 process system manufactured by Harms & Wende to perform refill FSSW. The welding procedure consists of preparation, plunge, dwell and retraction stages, and the welding parameters are summarized in Table S1. During welding, the temperature history was measured using K-type thermocouples, positioned at the AZ31B/DP600 interface underneath the clamping ring, see supplementary Figure 1(b_1). The surface appearance of the welds was measured using a Keyence 3D VR-5200 laser scanning microscope. The cross-sections of the welds were polished and examined by a FEI Quanta 650 field-emission scanning electron microscope (SEM) equipped with EDAX Apollo X energy dispersive X-ray spectroscopy (EDS) capability and Velocity electron backscatter diffraction (EBSD) system. Samples for transmission electron microscopy (TEM) were prepared by a focus ion beam (FIB), and the observations were conducted via a Thermo Fisher Talos F200 TEM. Moreover, the phases in the weld were identified by high-energy synchrotron X-ray diffraction (HEXRD) at P07B beamline, which is partly operated by the Helmholtz-Zentrum Hereon, of PETRA III, Deutsches Elektronen-Synchrotron (DESY). The LME crack in the weld was examined in transmission mode by a monochromatic X-ray beam with an energy of 87.1 keV and a size of 0.5 × 0.5 mm^2, see supplementary Figure S1. In order to understand the LME mechanism, a Gleeble-3500C thermal simulator was used to carry out hot tensile tests on the bare and Zn-coated AZ31B alloy. The Zn coating on the AZ31B alloy, see Figure S2, was produced by cold spray using a commercial high-pressure cold spray system (5/11, Impact Innovations, Germany). For details on the cold spray process, the interested reader is referred to our previous work [23]. The hot tensile tests were conducted at temperatures from 300 to 550°C with a heating rate of 200°C/s. After the target temperature was reached, a strain rate from 10^{-3} to 10^{-1} s^{-1} was applied.

The surface appearances of refill FSSW welds of Mg alloys to bare/galvanized steel are compared in Figure 1(c) and (d). With the presence of Zn coating, deep open cracks appeared on the surface, see Figure 1(d). SEM micrographs reveal that cracks are partially filled with a certain material, and eutectic structures are observed along the crack edges, as shown in Figure S3. Additionally, bulges were found near the small cracks on the surface of some joints welded under the same parameters (Figure S4(a)). The microstructure and chemical composition of these bulges were analyzed by SEM and EDS, as presented in Figure S4(b) and Table S2. The presence of a typical eutectic lamellar structure with high Zn content indicates the formation of a liquid Mg-Zn phase during welding.

In order to further understand the formation of the crack, the cross-section of the welds was characterized, see Figure 1(e). Deep cracks through the Mg alloy sheet are observed under the outer edge of the clamping ring (crack A), while there are still some short cracks under the clamping ring (crack B). The crack A is characterized by a lamellar coupled eutectic structure, consisting of eutectic α-Mg (dark region) and $Mg_{21}Zn_{25}$ (bright region) according to the results from EDS (Figure 1(g)) and HEXRD (Figure 1(h)). This eutectic structure indicates that liquid Mg-Zn phase filled in the crack during refill FSSW, and was transported from the weld interface toward the upper surface through the cracks under the combined effects of the clamping ring's downward force and thermal expansion, occasionally resulting in the formation of surface bulges when the cracks were relatively small, as shown in Figure S4. During cooling, the α-Mg and $Mg_{21}Zn_{25}$ were generated by eutectic reaction: $L \rightarrow \alpha\text{-Mg} + Mg_{21}Zn_{25}$ according to the Mg-Zn phase diagram [24]. The presence of liquid metal is a necessary condition for LME to occur, and it is also a typical characteristic of the LME phenomenon [25].

Except for the existence of liquid metal, another typical feature of LME is that the liquid metal penetrates grain boundaries and cracks occur in an intergranular

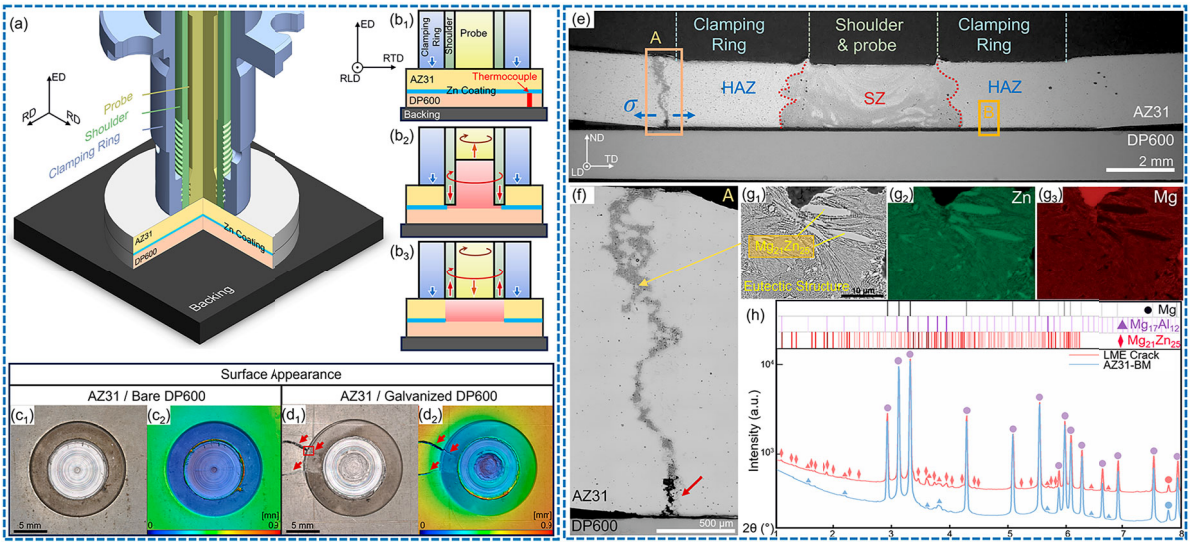

Figure 1. (a) Refill FSSW tool system and (b) procedure of refill FSSW, and surface appearance including (c_1, d_1) OM image and (c_2, d_2) height information of (c) Mg/bare steel weld and (d) Mg/galvanized steel weld with cracks marked by red arrows. (e) Cross section of AZ31/galvanized DP600 refill FSSW joint. (f) Enlarged image of the crack marked as region A in (e) with open crack marked by red arrow. (g) Eutectic microstructure locally filling the crack marked in (f) and its corresponding EDS maps of Zn and Mg, indicating the formation of liquid phase during refill FSSW. (h) Indexed HEXRD diffractograms of base AZ31 and crack, indicating the formation of the $Mg_{21}Zn_{25}$ phase in the crack.

fracture mode [26–28]. Therefore, a short crack at region B (Figure 1(e)) was characterized by EBSD. Figure 2 displays the distribution of grains and Zn content within region B to understand the propagation of the crack. The liquid Mg-Zn phase (brightest region) is mainly distributed at high angle (> 15 degree) grain boundaries (HAGBs), see Figure 2(a_2). Chemical composition line profile and mapping were carried out on regions I, II and III to further investigate the distribution of Zn element, as shown in Figure 2(d) and Figure S5. The Zn content in the region marked in Figure 2(b) is higher, indicating the Zn diffusion and concentration during welding in this region. It has been reported that HAGBs exhibit higher grain boundary energy [29,30], leading to a higher tendency of Zn penetration [31,32]. Combined with the grain morphologies, see Figure 2(c), it was found that the diffusion region of Zn extends through the HAGBs. Moreover, this region is positioned closer to the crack tip compared to the liquid Mg-Zn phase. This observation suggests that crack nucleation and propagation were initiated by Zn penetration along the HAGBs, followed by the melting of the Mg-Zn phase.

In order to further investigate the Zn concentration at HAGBs, TEM was carried out near the crack tip, as shown in Figure 3. The phase along the HAGB near the crack tip exhibits the highest Zn content (~ 50 at. %), and the diffusion layer with higher Zn content (~ 2 at. %) than base AZ31B alloy is also detected near the HAGB. The large phase and the thin phase (e and f in Figure 3(a)) at the HAGB are both distinguished as $Mg_{21}Zn_{25}$ by selected area electron diffraction (SAED) pattern and high-resolution TEM, respectively, see Figure 3(e) and (f). These results further indicate that crack nucleation and propagation started from Zn penetration at HAGBs and the subsequent Mg-Zn phase melting.

Another necessary condition for LME is the application of tensile stress [33,34]. During welding, the AZ31B sheet was bended at the outer edge of the clamping ring due to the downward pressure of the clamping ring and the increase in temperature during welding, see Figure 1(d) and (e), indicating that horizontal tensile stresses, σ, were applied on the crack nucleation position of the AZ31B sheet. These horizontal tensile stresses drove the LME crack propagation through the thickness of the Mg sheet.

Horizontal tensile stresses in the AZ31B sheet are likely to develop during the clamping and heating stages of the welding cycle. The downward compressive force exerted by the clamping ring induces lateral expansion in the sheet due to the Poisson effect, thereby generating radial tensile stresses. As the temperature increases and the material softens, the geometric constraints imposed by the clamping ring lead to localized bending deformation, which further induces both radial and circumferential tensile stresses in the bottom region surrounding the ring, consistent with the observed deformation behavior and the crack propagation direction shown in Figure 1(d) and (e). Further validation and quantitative analysis of the stress evolution is needed to confirm this hypothesis in future works.

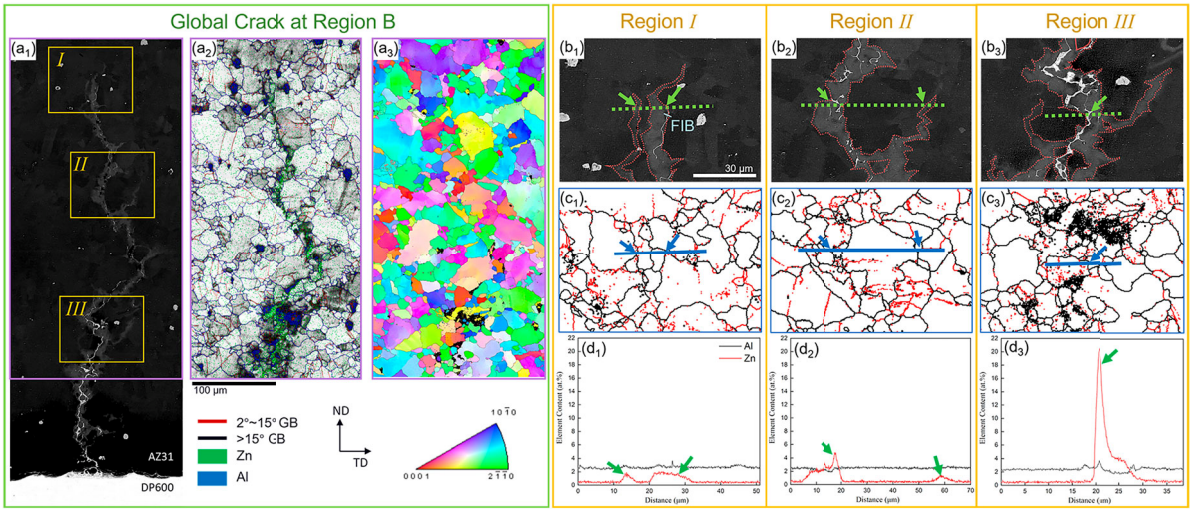

Figure 2. (a_1) Crack marked as region B in Figure 1(e), and (a_2) corresponding IQ map with low/high angle grain boundaries and distribution of Al and Zn, and (a_3) IPF map of the region marked in (a_1). (b) Microstructure and (c) corresponding low/high angle grain boundaries marked as regions I, II, and III in (a_1). The diffusion region of Zn is marked within red dash line. (d) EDS line profiles marked in (b). The concentration of Zn content marked by green arrows is located at HAGBs.

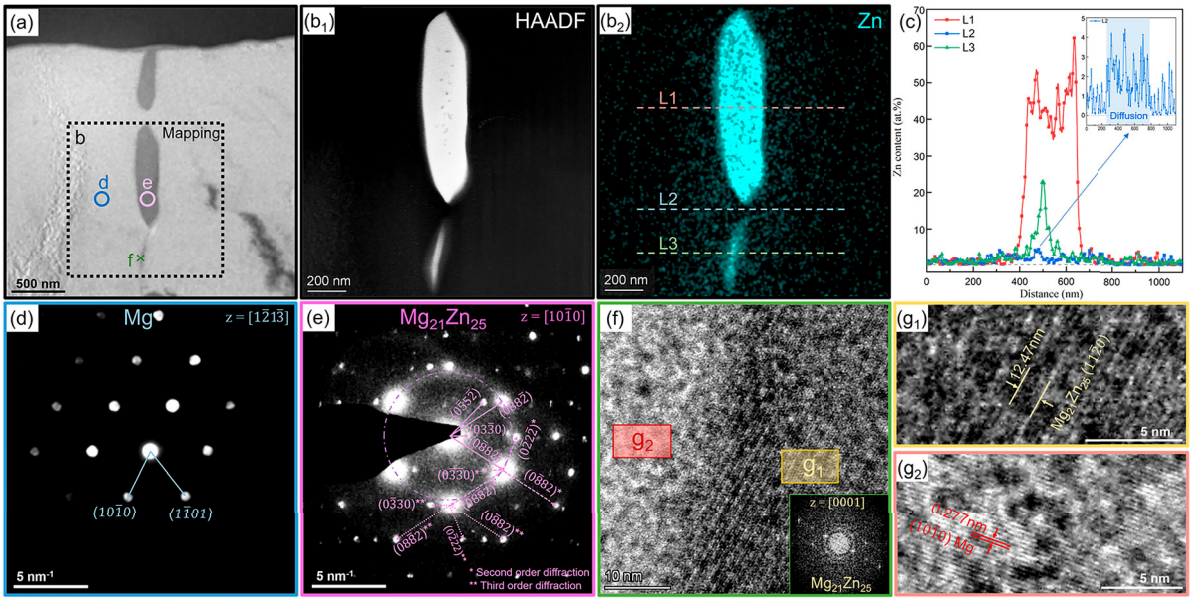

Figure 3. TEM results at the HAGB near the crack tip marked in Figure 2(b_1). (a) Bright-field image, (b_1) High-angle annular dark-field (HADDF) image and (b_2) EDS mapping of Zn marked in (a). (c) EDS line profiles marked in (b_2), indicating the Zn concentration at the HAGB. (d)–(e) selected area electron diffraction (SAED) patterns marked in (a), verifying the existence of $Mg_{21}Zn_{25}$ at HAGBs. (f) High-resolution TEM micrograph of the interphase area marked in (a). (g_1)–(g_2) High-resolution TEM micrograph labeled in (f).

In order to further understand the crack mechanism in refill FSSW of Mg/galvanized steel and to verify the LME phenomenon, the welding thermal cycle at the position near the crack nucleation was measured, see Figure 1(b_1) and Figure 4(a). During welding, the temperature increased significantly with a heating rate of about 150 ~ 200°C/s and reached about 360°C at the plunge stage, i.e. above the eutectic temperature of Mg-Zn phase (342°C). The temperature kept increasing during the dwell stage from 360 to 430°C, where the temperature decreased slightly from 430°C to about 360°C during the retracting stage. After welding, the temperature decreased significantly. During the whole welding procedure, the temperature underneath the clamping ring is maintained above the eutectic point for approximately 5 s, indicating the formation of liquid Mg-Zn phase. Furthermore, the temperatures within the shoulder and probe regions can be assumed even higher as shown in numerical simulations of refill FSSW [35].

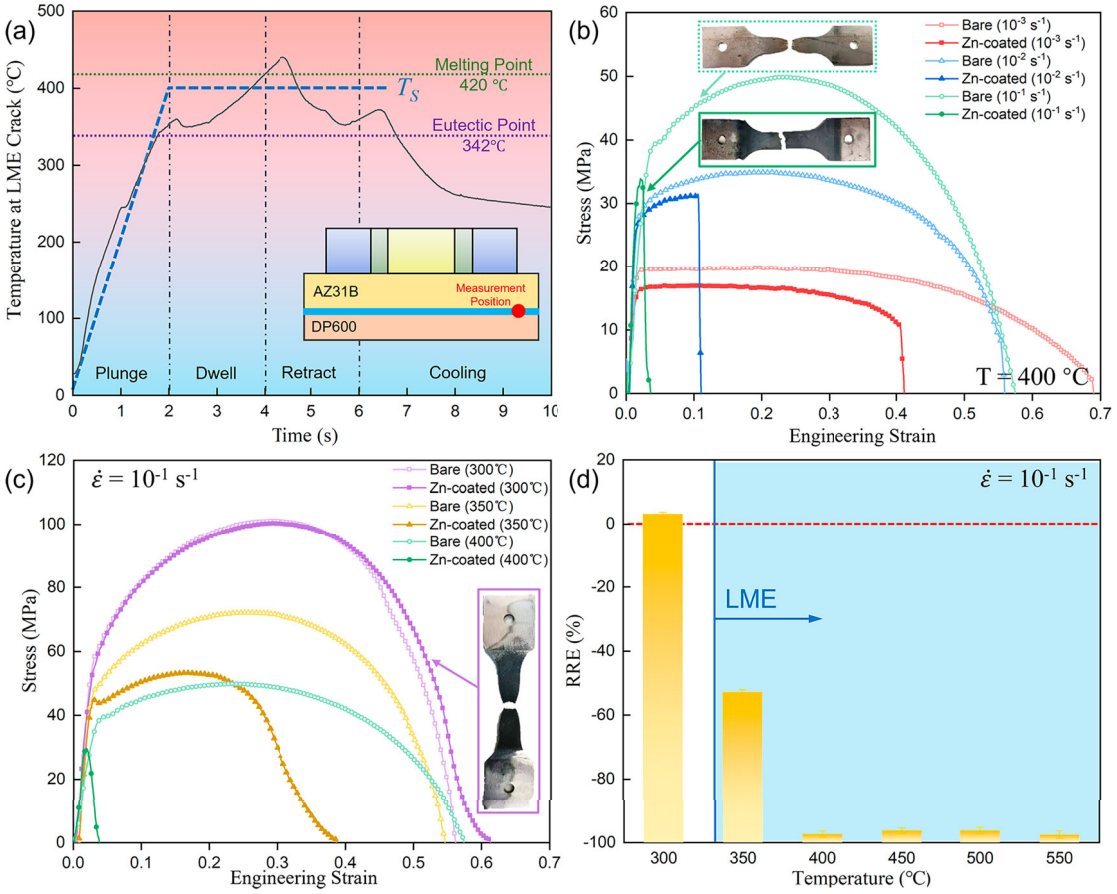

Figure 4. (a) Thermal cycle during refill FSSW as well as the simulated temperature history in hot tensile test, T_S. (b) Engineering Stress–Strain curve of bare/Zn coated AZ31B alloy in hot tensile test with peak temperature of 400°C at different strain rates (10^{-3}, 10^{-2}, and 10^{-1} s^{-1}). (c) Stress–Strain curve of bare/Zn-coated AZ31B alloy in hot tensile test at a strain rate of 10^{-1} s^{-1} at different peak temperatures. (d) Relative reduction of energy (RRE) at different peak temperatures, indicating that LME occurs at temperatures above 350°C.

Hot tensile tests are usually used to identify the occurrence of LME and investigate the conditions of the LME phenomenon [36,37]. At first, the hot tensile test simulating the condition of welding was carried out at a peak temperature of 400°C at different strain rates (10^{-3}, 10^{-2}, and 10^{-1} s^{-1}) on the bare and Zn-coated Mg alloy, see Figure 4(b). The ductility of the Zn-coated AZ31B Mg alloy was severely reduced compared with that of the bare AZ31B Mg alloy. The fracture mode changes from ductile fracture with necking characteristics to brittle fracture due to the effects of Zn coating. The typical brittle intergranular fracture morphology of Zn-coated samples with higher Zn content, see Figure S7, further verified the occurrence of the LME phenomenon [38]. Additionally, the increase of the strain rate also enhanced the reduction of ductility of the Zn-coated Mg.

Hot tensile tests at different temperatures were also carried out to investigate the occurrence conditions of LME phenomenon on Zn coating Mg alloy. The relative reduction of energy (RRE) was calculated to determine the occurrence of LME [39]. At 300°C (below the eutectic temperature of Mg-Zn phase), the Zn-coated AZ31B Mg alloy exhibited similar mechanical behavior and ductility with ductile fracture compared to the bare AZ31B Mg alloy, and the RRE is near 0. As the temperature increased above the eutectic temperature of the Mg-Zn phase, the Mg-Zn phase melted and the ductility of Zn-coated AZ31B Mg alloy decreased significantly, further indicating the presence of melting Mg-Zn phase, which led to the occurrence of LME.

The identification of the penetration of Zn and the subsequent formation of liquid Mg-Zn phase (Figures 3 and 4), as well as the temperature of LME occurrence (Figure 4) allow to develop a hypothesis for a possible LME mechanism in refill FSSW of Mg/galvanize steel. At the plunge stage of refill FSSW, the increasing temperature softens the Mg alloy under the clamping ring. Then the Mg alloy bends and a tensile stress is induced at the outer clamping ring due to the compression. At the same time, the mutual diffusion of Zn and Mg at the interface

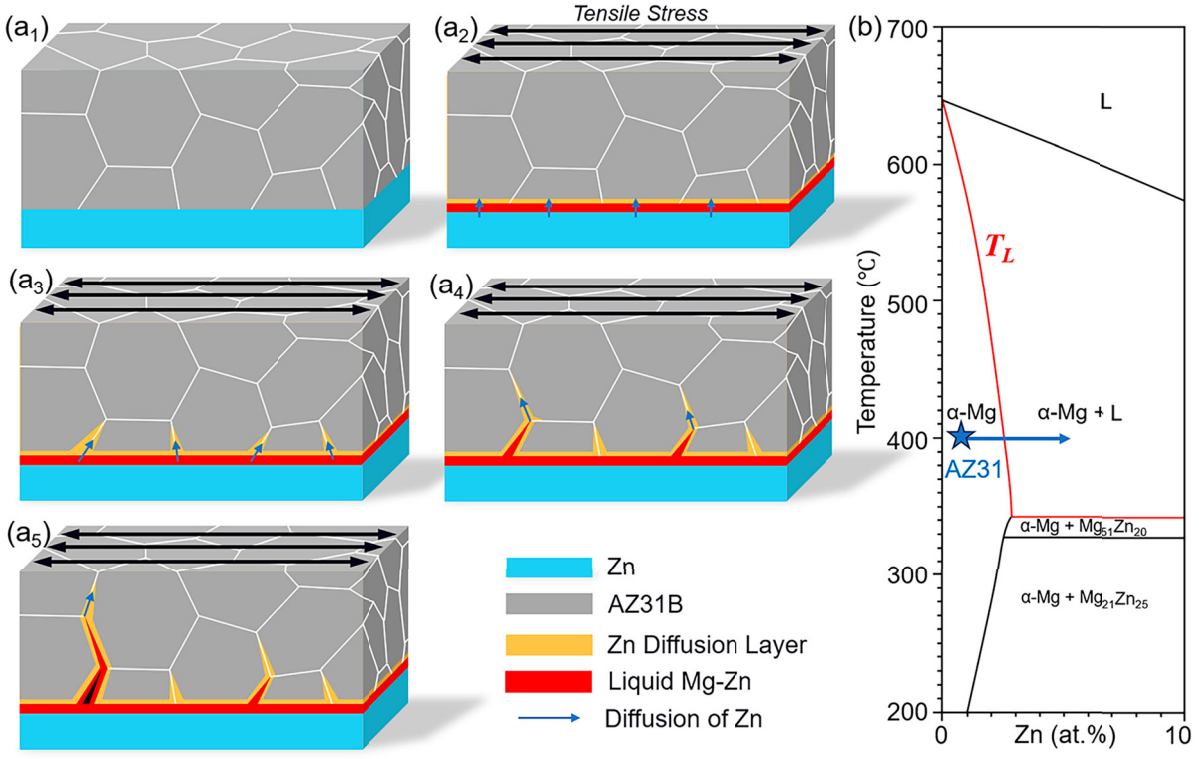

Figure 5. (a_1)–(a_5) Possible LME mechanism model for Refill FSSW of Mg/galvanize steel. (b) Mg-Zn phase diagram with Zn diffusion.

between Zn coating and upper Mg sheet is enhanced due to the increasing temperature, and Mg-Zn melts when the temperature reaches its eutectic temperature (Figure 5(a_2)). As the welding process progresses, due to the formation of liquid Mg-Zn phase and the application of tensile stresses, the Zn atoms prefer to diffuse at the HAGBs in the Mg alloy (Figure 5(a_3)). The penetration of Zn increases the local Zn content at HAGBs and reduces the liquidus temperature of the Mg alloy, T_L, see Figure 5(b). With the diffusion of Zn, the Mg alloy with higher Zn content at GBs starts to melt when T_L is below the processing temperature, and the liquidus Mg-Zn phase subsequently stimulates the penetration of further Zn into subsequent HAGBs (Figure 5(a_4)). With the penetration of Zn atoms and propagation of liquid Mg-Zn phase at Mg HAGBs, LME crack initiates at the interface between Zn and the Mg alloy, and propagates along the HAGBs in the Mg alloy (Figure 5(a_5)), presenting a decrease of ductility of the Mg alloy at high temperature.

In currently well-studied Zn-containing systems susceptible to LME, such as the Fe-Zn system, there are no eutectic points below the melting temperature of pure Zn [10]. According to Fe-Zn phase diagram, as the Zn content increases from 0% to 42 at.%, the onset of partial melting decreases from 1538 to 782°C, which is still substantially higher than the melting point of pure Zn. Therefore, grain boundaries enriched with Zn in the Fe matrix generally do not liquefy within a short period. Instead, the diffusion of Zn atoms may lead to the formation of brittle intermetallic Γ-phase along the grain boundaries [3], causing grain boundary embrittlement. Under applied tensile stress, these embrittled grain boundaries are prone to cracking. Subsequently, the liquid Zn may infiltrate into the crack tip, promoting further crack propagation [35]. In such systems, higher temperatures and strain rates are typically required to maintain the presence of a liquid phase, which facilitates the initiation and propagation of LME. In contrast, in the Mg-Zn system, when the Zn content increases to just 2.4 at.%, the onset temperature for partial melting drops to approximately 342°C, which is below the melting point of pure Zn. This significantly enhances the tendency for liquefaction of Zn-enriched grain boundaries. The presence of a stable liquid phase at the crack tip increases the susceptibility to rapid and sustained LME crack propagation, even under relatively low temperatures and strain rates.

Based on the experimental results and the developed LME mechanism model, two potential strategies are proposed to prevent the occurrence of LME cracks: (i) Decreasing the heat input during refill FSSW, such as decreasing the rotational speed. When the temperature beneath the clamping ring is kept below the eutectic temperature of the Mg-Zn phase, one of the necessary conditions, i.e. the formation of liquid phase, will be prevented; (ii) Minimizing bending of the Mg sheet and of

the horizontal tensile stresses in the Mg, such as decreasing the welding force or increasing the diameter of the clamping ring, since the tensile stress is another necessary condition of LME. Refill FSSW of Mg/galvanized steel using different welding parameters has been carried out, as shown in Table S3, which preliminarily verifies that these potential strategies could prevent the occurrence of LME cracks.

In summary, LME phenomenon, characterized by the presence of liquid phase at HAGBs and intergranular crack, was discovered in refill FSSW of Mg/galvanized steel for the first time. The nucleation and propagation of the LME crack are driven by the penetration of Zn at Mg HAGBs under tensile stresses and the subsequent formation of liquid Mg-Zn phase. Therefore, decreasing heat input and horizontal tensile stresses are potential strategies to avoid LME cracks in refill FSSW of Mg/galvanized steel.

Acknowledgments

The authors acknowledge the financial support of the National Natural Science Foundation of China (grant number 52405386) and State Key Laboratory of Precision Welding & Joining of Materials and Structures (grant number MSWJ-24M13). The TEM experiment was funded by 'Project 2025HWYQ-005 supported by Shandong Provincial Natural Science Fund for Excellent Young Scientists Fund Program (Overseas)'. We acknowledge DESY (Hamburg, Germany), a member of the Helmholtz Association HGF, for the provision of experimental facilities. Parts of this research were carried out at the P07 beamline which is partly operated by the Helmholtz-Zentrum Hereon at PETRA III. The authors are grateful to Mr. Günter Meister from Helmholtz-Zentrum Hereon, Institute of Metallic Biomaterials, for the provision of the base materials used in this study. The technical support of Mr. Menno Peters from Helmholtz-Zentrum Hereon, Institute of Material and Process Design during this work is gratefully acknowledged.

Disclosure statement

No potential conflict of interest was reported by the author(s).

Funding

This work was supported by National Natural Science Foundation of China [grant number 52405386]; State Key Laboratory of Precision Welding & Joining of Materials and Structures [grant number MSWJ-24M13]; Shandong Provincial Natural Science Fund for Excellent Young Scientists Fund Program (Overseas) [grant number 2025HWYQ-005].

References

[1] Monchoux J, Rabkin E. Microstucture evolution and interfacial properties in the Fe–Pb system. Acta Mater. 2002;50(12):3161–3176. doi:10.1016/S1359-6454(02)00129-5

[2] Cho L, Kang H, Lee C, et al. Microstructure of liquid metal embrittlement cracks on Zn-coated 22MnB5 press-hardened steel. Scr Mater. 2014;90-91:25–28. doi:10.1016/j.scriptamat.2014.07.008

[3] Ikeda Y, Ni H, Chakraborty A, et al. Segregation-induced grain-boundary precipitation during early stages of liquid-metal embrittlement of an advanced high-strength steel. Acta Mater. 2023;259:119243. doi:10.1016/j.actamat.2023.119243

[4] Naderi M, Peterlechner M, Schafler E, et al. Kinetic, volumetric and structural effects induced by liquid Ga penetration into ultrafine grained Al. Acta Mater. 2015;99:196–205. doi:10.1016/j.actamat.2015.07.061

[5] Nam H-S, Srolovitz DJ. Effect of material properties on liquid metal embrittlement in the Al–Ga system. Acta Mater. 2009;57(5):1546–1553. doi:10.1016/j.actamat.2008.11.041

[6] Senel E, Walmsley JC, Diplas S, et al. Liquid metal embrittlement of aluminium by segregation of trace element gallium. Corros Sci. 2014;85:167–173. doi:10.1016/j.corsci.2014.04.012

[7] Kundu A, Asl KM, Luo J, et al. Identification of a bilayer grain boundary complexion in Bi-doped Cu. Scr Mater. 2013;68(2):146–149. doi:10.1016/j.scriptamat.2012.10.012

[8] Schweinfest R, Paxton AT, Finnis MW. Bismuth embrittlement of copper is an atomic size effect. Nature. 2004;432(7020):1008–1011. doi:10.1038/nature03198

[9] Marie N, Wolski K, Biscondi M. Intergranular penetration and embrittlement of solid nickel through bismuth vapour condensation at 700°C. J Nucl Mater. 2001;296(1-3):282–288. doi:10.1016/S0022-3115(01)00530-X

[10] Razmpoosh M, DiGiovanni C, Zhou Y, et al. Pathway to understand liquid metal embrittlement (LME) in Fe-Zn couple: From fundamentals toward application. Prog Mater Sci. 2021;121:100798. doi:10.1016/j.pmatsci.2021.100798

[11] Beal C, Kleber X, Fabregue D, et al. Liquid zinc embrittlement of a high-manganese-content TWIP steel. Philos Mag Lett. 2011;91(4):297–303. doi:10.1080/09500839.2011.559177

[12] Ashiri R, Shamanian M, Salimijazi HR, et al. Liquid metal embrittlement-free welds of Zn-coated twinning induced plasticity steels. Scr Mater. 2016;114:41–47. doi:10.1016/j.scriptamat.2015.11.027

[13] Shao CW, Zhang P, Wang XG, et al. High-cycle fatigue behavior of TWIP steel with graded grains: breaking the rule of mixture. Mater Res Lett. 2019;7(1):26–32. doi:10.1080/21663831.2018.1550822

[14] Kim YG, Kim IJ, Kim JS, et al. Evaluation of surface crack in resistance spot welds of Zn-coated steel. Mater Trans. 2014;55(1):171–175. doi:10.2320/matertrans.M2013244

[15] Song S, Shojaee M, Midawi A, et al. Influence of expulsion and heat extraction resulting from changes to electrode force on liquid metal embrittlement during resistance spot welding. J Mater Res Technol. 2023;23:1458–1470. doi:10.1016/j.jmrt.2023.01.093

[16] Lalachan A, Murugan SP, Jin WS, et al. Liquid metal embrittlement in Zn-coated steel resistance spot welding: Critical electrode-contact and nugget growth for stress development and cracking. J Mater Process Technol. 2023;318:118009. doi:10.1016/j.jmatprotec.2023.118009

[17] Ina K, Koizumi H. Penetration of liquid metals into solid metals and liquid metal embrittlement. Mater Sci Eng A. 2004;387-389:390–394. doi:10.1016/j.msea.2004.05.042
[18] Edalati K, Bachmaier A, Beloshenko VA, et al. Nanomaterials by severe plastic deformation: review of historical developments and recent advances. Mater Res Lett. 2022;10(4):163–256. doi:10.1080/21663831.2022.2029779
[19] Zhan R, Liu Q, Li X, et al. Achieving the targeted regulation of gamma prime phase in the heterogeneous friction weld of highly alloyed nickel-based superalloy by electric current treatment. Mater Res Lett. 2025;13(6):642–648. doi:10.1080/21663831.2025.2492349
[20] Li L, Tan C, Chen Y, et al. Comparative study on microstructure and mechanical properties of laser welded–brazed Mg/mild steel and Mg/stainless steel joints. Mater Des. 2013;43:59–65. doi:10.1016/j.matdes.2012.06.057
[21] Liu Y, Yu D, Zhang Y, et al. Research advances on weldability of Mg alloy and other metals worldwide in recent 20 years. J Mater Res Technol. 2023;25:3458–3481. doi:10.1016/j.jmrt.2023.06.184
[22] Fu B, Shen J, Suhuddin UF, et al. Revealing joining mechanism in refill friction stir spot welding of AZ31 magnesium alloy to galvanized DP600 steel. Mater Des. 2021;209:109997. doi:10.1016/j.matdes.2021.109997
[23] Huang C, Chen T, Fu B, et al. Ductility and fracture behavior of cold spray additive manufactured zinc. Addit Manuf. 2024;89(5):104310.
[24] Okamoto H. Supplemental literature review of binary phase diagrams: Cs-In, Cs-K, Cs-Rb, Eu-In, Ho-Mn, K-Rb, Li-Mg, Mg-Nd, Mg-Zn, Mn-Sm, O-Sb, and Si-Sr. J Phase Equilib Diffus. 2013;34(3):251–263. doi:10.1007/s11669-013-0233-2
[25] Ling Z, Chen T, Kong L, et al. Liquid metal embrittlement cracking during resistance spot welding of galvanized Q&P980 steel. Metall Mater Trans A. 2019;50:5128–5142. doi:10.1007/s11661-019-05388-6
[26] Razmpoosh MH, Biro E, Chen DL, et al. Liquid metal embrittlement in laser lap joining of TWIP and medium-manganese TRIP steel: the role of stress and grain boundaries. Mater Charact. 2018;145:627–633. doi:10.1016/j.matchar.2018.09.018
[27] Akbari E, Kürnsteiner P, Steineder K, et al. Insight into grain boundaries with reduced liquid metal embrittlement susceptibility in a boron-added 3rd generation advanced high strength steel. Mater Des. 2024;237:112584. doi:10.1016/j.matdes.2023.112584
[28] Razmpoosh M, Langelier B, Marzbanrad E, et al. Atomic-scale investigation of liquid-metal-embrittlement crack-path: revealing mechanism and role of grain boundary chemistry. Acta Mater. 2021;204:116519. doi:10.1016/j.actamat.2020.116519
[29] Ludwig W, Pereiro-López E, Bellet D. In situ investigation of liquid Ga penetration in Al bicrystal grain boundaries: grain boundary wetting or liquid metal embrittlement? Acta Mater. 2005;53(1):151–162. doi:10.1016/j.actamat.2004.09.012
[30] Xue HT, Zhang ZJ, Hu ZL, et al. Twinning-induced energy-lowering structural transformation of Σ5 [001](210) grain boundary: A pathway to grain-boundary relaxation. Acta Mater. 2025;288:120829. doi:10.1016/j.actamat.2025.120829
[31] Scheiber D, Prabitz K, Romaner L, et al. The influence of alloying on Zn liquid metal embrittlement in steels. Acta Mater. 2020;195:750–760. doi:10.1016/j.actamat.2020.06.001
[32] Razmpoosh M, Macwan A, Goodwin F, et al. Role of random and coincidence site lattice grain boundaries in liquid metal embrittlement of iron (FCC)-Zn couple. Metall Mater Trans A. 2020;51:3938–3944. doi:10.1007/s11661-020-05857-3
[33] Rajagopalan M, Bhatia M, Tschopp M, et al. Atomic-scale analysis of liquid-gallium embrittlement of aluminum grain boundaries. Acta Mater. 2014;73:312–325. doi:10.1016/j.actamat.2014.04.011
[34] Gordon P, An HH. The mechanisms of crack initiation and crack propagation in metal-induced embrittlement of metals. Metall Trans A. 1982;13:457–472. doi:10.1007/BF02643354
[35] Janga VSR, Awang M, Yamin MF, et al. Experimental and numerical analysis of refill friction stir spot welding of thin AA7075-T6 sheets. Materials (Basel). 2021;14(23):7485. doi:10.3390/ma14237485
[36] Beal C, Kleber X, Fabregue D, et al. Liquid zinc embrittlement of twinning-induced plasticity steel. Scr Mater. 2012;66(12):1030–1033. doi:10.1016/j.scriptamat.2011.12.040
[37] Kang JH, Hong SH, Kim J, et al. Zn-induced liquid metal embrittlement of galvanized high-Mn steel: strain-rate dependency. Mater Sci Eng A. 2020;793:139996. doi:10.1016/j.msea.2020.139996
[38] Ghatei-Kalashami A, Khan MS, Goodwin F, et al. Investigating the mechanism of zinc-induced liquid metal embrittlement crack initiation in austenitic microstructure. J Mater Sci. 2023;58(39):15314–15335. doi:10.1007/s10853-023-08963-w
[39] Ling Z, Wang M, Kong L, et al. Towards an explanation of liquid metal embrittlement cracking in resistance spot welding of dissimilar steels. Mater Des. 2020;195:109055. doi:10.1016/j.matdes.2020.109055